Pergamon

Bioorganic & Medicinal Chemistry 10 (2002) 2471–2478

BIOORGANIC & MEDICINAL CHEMISTRY

Computer-Aided Simulation of a Dendrimer with a Protoporphyrinic Core as Potential, Novel Hemoprotein Mimic

Maurizio Fermeglia, Marco Ferrone and Sabrina Pricl*

Computer-aided Systems Laboratory, Department of Chemical Engineering—DICAMP, University of Trieste, Piazzale Europa 1, 34127 Trieste, Italy

Received 4 January 2002; revised 22 March 2002; accepted 3 April 2002

Abstract—In this work, we have inserted the ion-heme group characterizing human blood in a class of synthetic, dendrimeric macromolecules, to evaluate a series of structural and physico-chemical properties related to the possible biological activity of these polymers. To this purpose, we have performed a complete series of investigations of five dendrimer generations both in vacuum and in water by molecular mechanics/dynamics simulations. To mimic oxygen binding, we have studied the same molecules in which the protoporphyrinic core was complexed to a Fe(II)–O_2–hystidine residue. The main results of this study have led us to conclude that all dendrimer generations can bind oxygen stably, the fifth generation being the most affine to the myoglobin molecule, the natural carrier of blood oxygen. © 2002 Published by Elsevier Science Ltd.

Introduction

As a new class of materials, dendrimers (or starburst polymers) have recently awakened great interest in the scientific community. Despite the substantial difficulties encountered in their synthesis, a wide range of these substances have been produced and, although only in part, characterized.[1–4] Starburst dendrimers possess three major architectural components: an initiator core, an interior and an exterior (see Fig. 1). By definition or construction, these three components are interdependent and reflect a unique molecular genealogy. As we progress from the initiator core to an advanced dendrimer stage (or *generation*), this molecular genealogy manifests itself in a variety of ways. Just as we can trace ancestry and lineage in higher organisms, so one can observe a molecular-level parallel by thinking of these transformations in the context of:

- stored molecular information at each dendrimer stage; and
- molecular information transferred to the progeny dendrimer surface at each transformation.

Thus, beginning with the core, molecular details are sequentially transcribed and stored to produce interior and, ultimately, exterior features which are characteristic of that dendrimer family. A liaison with some kind of primitive abiotic gene is then quite evident. In this fashion, interior features such as size, chemical composition, flexibility and topology are developed and manifested as stored molecular information. The interior of a

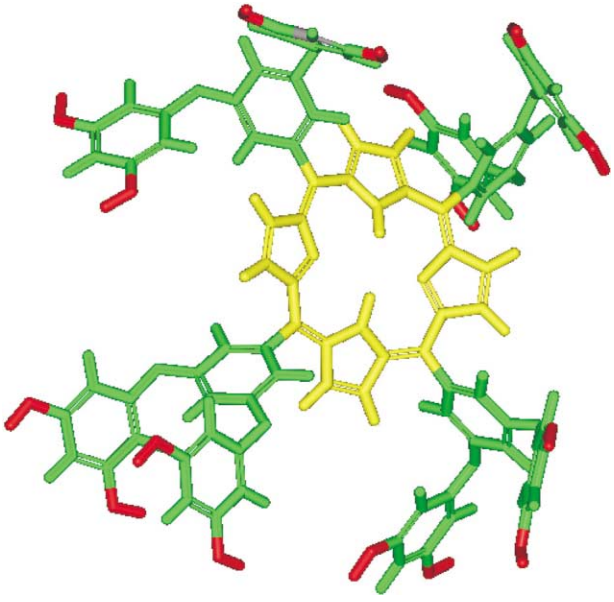

Figure 1. Major architectural components of a dendrimer molecule: initiatior core (yellow), interior (blue) and exterior (red).

*Corresponding author. Tel.: +39-04-0676-3750; fax: +39-04-056-9823; e-mail: sabrinap@dicamp.units.it

0968-0896/02/$ - see front matter © 2002 Published by Elsevier Science Ltd.
PII: S0968-0896(02)00117-7

dendrimer consists of a scaffold upon which surface properties such as shape, reactivity, stoichiometry, congestion, special kinetic features, flexibility and fractal character can be generated and controlled. These surface features may reflect in several interesting attributes, such as divergent recognition[5] and exo-reception properties,[6] which find an analogy in biological processes like, for instance, antibody-antigen recognition[7] and protein–protein interactions.[8]

Now, in mimicking biological functions of hemoproteins, one of the attractive targets is to realize the reversible dioxygen binding activities of hemoglobin and myoglobin.[9] To this purpose, a variety of sterically hindered iron porphyrins have been synthesized,[10–14] some of which indeed form stable dioxygen adducts but only under anhydrous conditions. On the other hand, in aqueous media, successful examples have been limited to only iron picket-fence porphyrins embedded within a synthetic bilayer membrane.[15] Quite recently, Jin et al.[16] have synthesized a series of aryl ether dendrimers bearing porphyrin functionality as a core. Their experimental characterization has shown that the interior porphyrins functionality is almost encapsulated when the number of aromatic layers in the dendrimer framework is higher than four. Due to the sterical and hydrophobic protection around the active site, a large dendrimer iron porphyrin has been verified to show a dioxygen binding activity, similar to hemoglobin.[9]

All these application potentials, however, will not be realized before the understating of their physical properties is considerably advanced. Therefore, in our attempt of exploring in greater detail the underlying mechanism at the basis of the potential biological functions of these synthetic, complex macromolecules, we performed a comprehensive characterization by computer-aided simulations of the protoporphyrinic group covalently encapsulated within up to five-generation aryl ether dendrimer cages as the first monomolecular

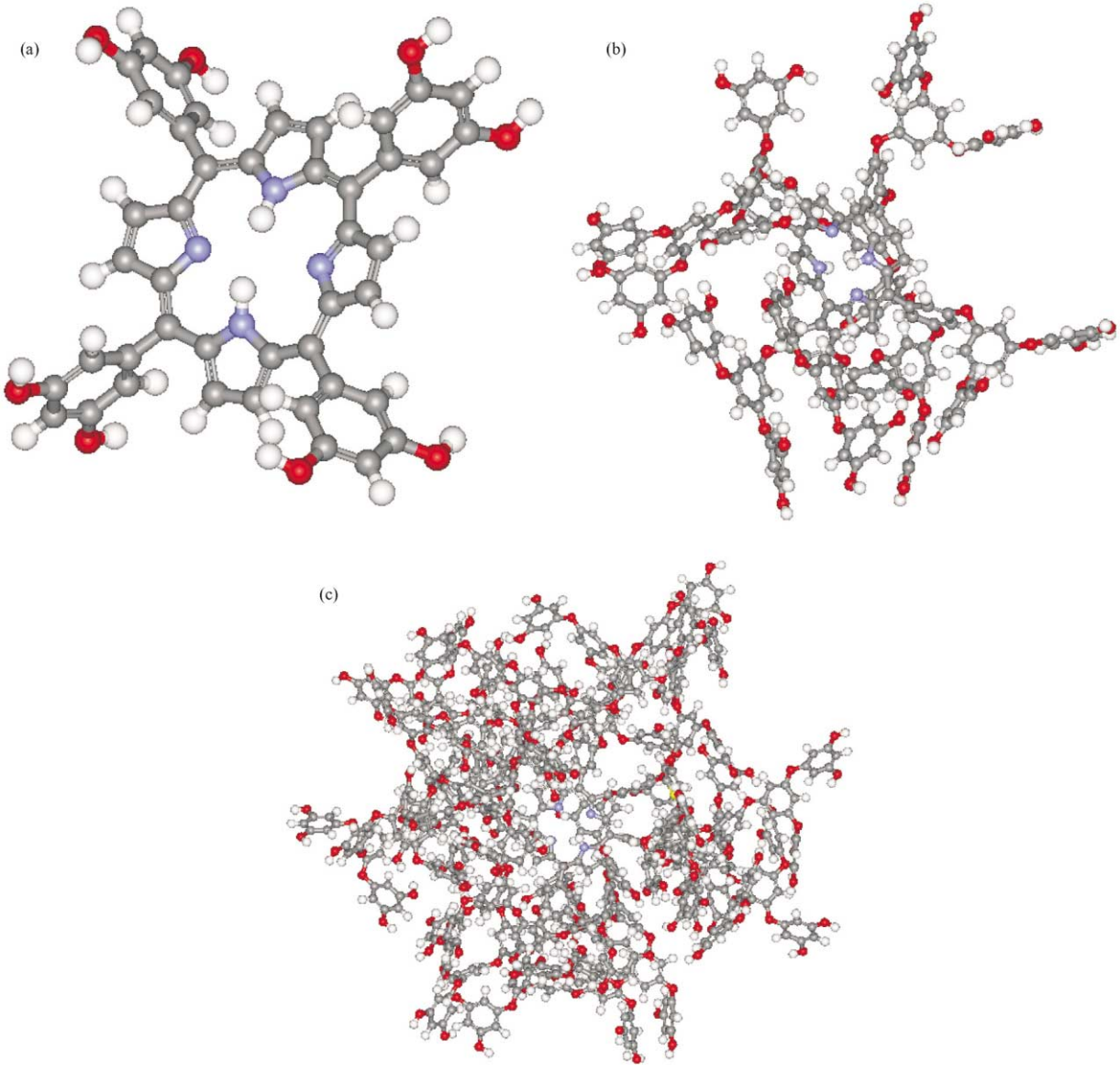

Figure 2. Molecular models of generation 1 (a), 3 (b) and 5 (c) for the iron protoporphyrin-based dendrimer.

model of dioxygen-carrying hemoprotein. The dendrimeric protoporphyrins have been studied both as isolated molecules and in a solvated environment; further, the influence on the relevant properties has been investigated both for the dendrimers with an empty protoporphyrinic core ($dend_E$) and for those carrying a Fe(II)–dioxygen–hystidine (Fe–O_2–Hys) complex coordinated to the protoporphyrin nucleus ($dend_C$).

There are several reasons that have prompted us to adopt this particular approach that involved an extensive series of molecular mechanics/dynamics simulations; suffice here to mention that, nowadays, the quality of the results obtained by virtual experiments parallels that achievable in the real laboratory and, no less important, long time scales and very high costs are needed to prepare defect-free dendrimers with a high generation number.

Results and Discussion

Figure 2a–c shows the molecular models of generation 1, 3 and 5 for the iron protoporphyrin-based dendrimers obtained as a result of the first structural investigations performed with MD simulations under NVT conditions. If the first generation is quite open, by generation 3 the dendrimers have already reached the conformation of a tangled mass. In accordance to the NMR evidences of Jiang and Aida,[9] the analysis of our computer simulations reveals that, by generation 5, the protoporphyrinic core is well embedded into the dendrimeric shell, which can thus act as a sterical and hydrophobic protection for dioxygen binding activity. As we can evidence from Figure 2, our calculations indicate a dramatic change in morphology with generation; indeed, the early generations (G1–G3) are highly asymmetric, whereas generations G4–G5 are nearly spherical.

This transition to a spheroidal form can be quantified by the aspect ratio of principal moments of inertia for various generations G of the dendrimer with an empty protoporphyrinic core (see Fig. 3). The main aspect ratio (I_x/I_z) decreases from 3.4 to 1.2, the I_z/I_y ratio increases from 0.29 up to 0.91, whereas I_y/I_x is characterized by a constant value of 1 through all generations, as the square planar, rigid protoporphyrinic nucleus does not undergo considerable distortions as the number of lateral ramifications increases. The alternative case of the protoporphyrin nucleus complexed with a Fe(II)–O_2–hys assembly presents an almost analogous situation, except for the slight, quantitative increase in the values of the two aspect ratios I_x/I_z and I_z/I_y for the first dendrimer generations, where the linear dimension of the Fe–O_2–Hys complex (11.5 Å) partially hinders the close packing of the dendrimer branches. The conformational change described above has been verified for other dendrimeric series characterized by quite different functionalities such as, for instance, poly(propylene imine) (both NH_2 and CN terminated)[17] and poly(β-alanine).[18]

The radius of gyration R_g is a fundamental tool for the characterization of the structural properties of dendrimers. This quantity is defined as the square root of the second invariant of the first order tensor **S**, which accounts for the spatial distribution of the atom chains by mediating over all N molecular components. The R_g values estimated by molecular dynamics simulations for all generations of $dend_E$ and $dend_C$ molecules are plotted in Figure 4 as a function of the molecular weight M_r. Again, no major distinctions can be observed between the two molecular series; in particular, the linear relation between log R_g and log M_r is a further indication for a compact space filling structures with fractal dimensionality d_f of about 2.8 in the case of $dend_E$ and 2.6 in the case of $dend_C$, respectively.

Fractal geometry is a mathematical tool for dealing with complex systems that have no characteristic length scales. Scale-invariant systems are usually characterized by non-integer (i.e., fractal) dimensions, and hence the objective of any fractal analysis is to find a relationship of some kind of power-law:

$$\text{physical property} \propto \text{variable}^{\text{scaling exponent}} \quad (1)$$

where the variable and the exponent are related to the fractal dimension. This relation is obviously one that can cover a very broad range of molecular structures;

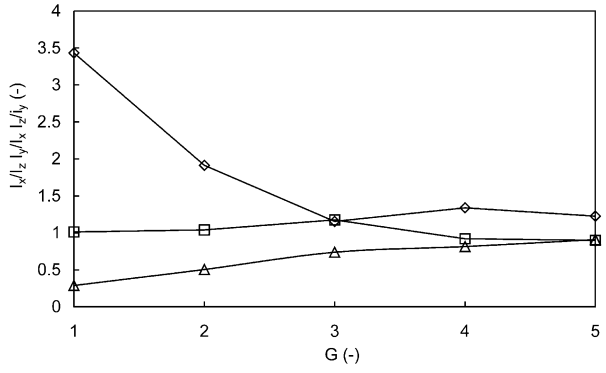

Figure 3. Aspect ratio of the principal moments of inertia for various $dend_E$ generations: I_x/I_z (◇); I_y/I_z (□); I_z/I_y (△) (lines serve as guide for the eye).

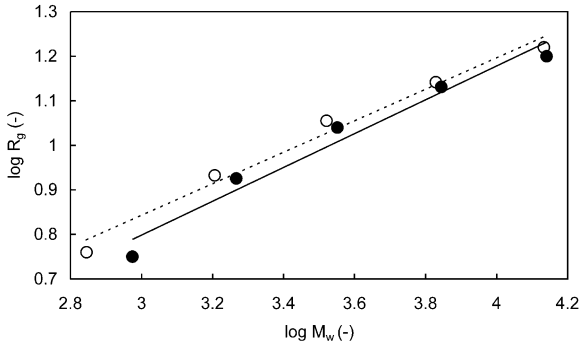

Figure 4. Relationship between radius of gyration R_g and molecular weight M_r for both dendrimeric series. $dend_E$: calculated values (○); best fit (—). $dend_C$: calculated values (●); best fit (—).

however, this kind of power law requires some symmetry in these structures. Interestingly enough, the values of d_f calculated for both dendrimeric series considered in this work are close to the average mass fractal dimension exhibited by the vast majority of proteins,[19] that is 2.7, and to the exponent characterizing the distribution of masses of an ideally branched polymer ($d_f = 2.5$). Arteries and veins in mammalian vascular systems, too, have been found to obey the scaling law (1) over a range of 20 bifurcations between heart and capillaries. Estimates of the relevant scaling exponent[20] give values again near 2.7. This is a reasonable value for biological evolution to have attained, given the requirement that arteries and veins should come close to every point of the body that needs nourishment and waste disposal. But the ideal value of $d_f = 3$ for this purpose is, of course, unattainable, because a space-filling vascular system leaves too little tissue for other tasks.

One of the important problems in structural biology is the origin of specificity and recognition in molecular interactions. An essential step in this process is complementary contact between approaching molecular surfaces. Surface representations of macromolecules such as, in our specific case, proteins or dendrimers, have provided a powerful approach for characterizing the structure, folding, interactions and properties of such molecules. A fundamental feature of surfaces that has not been characterized by these representations, however, is the texture (or roughness) of polymer surfaces, and its role in molecular interactions has not been defined. The degree of irregularity of a surface may be described[21] by means of another fractal dimension D. As a surface becomes more irregular, the corresponding fractal dimension increases, starting from its lower limiting value $D = 2$, corresponding to an entirely smooth surface. In this case, the value of D may be obtained from the slope of the log(surface area) against log(probe size) used by the Connolly algorithm (see Computational details) to determine the molecular surface as follows:

$$2 - D = \frac{\mathrm{dlog}(A_S)}{\mathrm{dlog}(R_p)} \qquad (2)$$

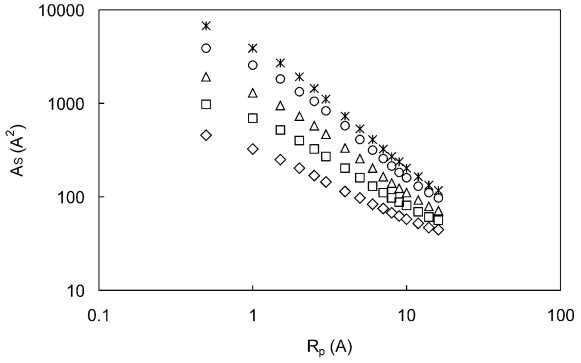

Figure 5. Double logarithmic plot of the molecular surface area A_s versus probe radius R_p for the five generations of dend$_E$: G1 (◇); G2 (□); G3 (△); G4 (○); G5 (∗).

where A_S and R_p are the molecular surface area and probe radius, respectively. Such a relationship is illustrated in Figure 5 for the five generations of the dendrimer with an empty protoporphyrinic core. As we may infer from this graph, the slopes of these plots show a tendency to reach a plateau (corresponding to $D = 2$) in the limit of both small and large probe sizes. Small probes predominantly interact with the smooth van der Waals spheres describing the dendrimer atoms, whereas large probes are sensitive to the overall shape of the molecule. For probes in the intermediate range (i.e., 1–10 Å), however, the value of D progressively increases with increasing G from 2.7 to 3.2, with an average value of 3.0. Since this probe radius size range corresponds to the approximate size of water molecules and side chains, such probes should be sensitive to specific interactions between residues. The same analysis has been performed on the myoglobin molecule for comparison (entry 1MBD[22] in the Protein Data Bank[23]) and the corresponding fractal dimension is indeed equal to that of G5, that is $D = 3.2$.

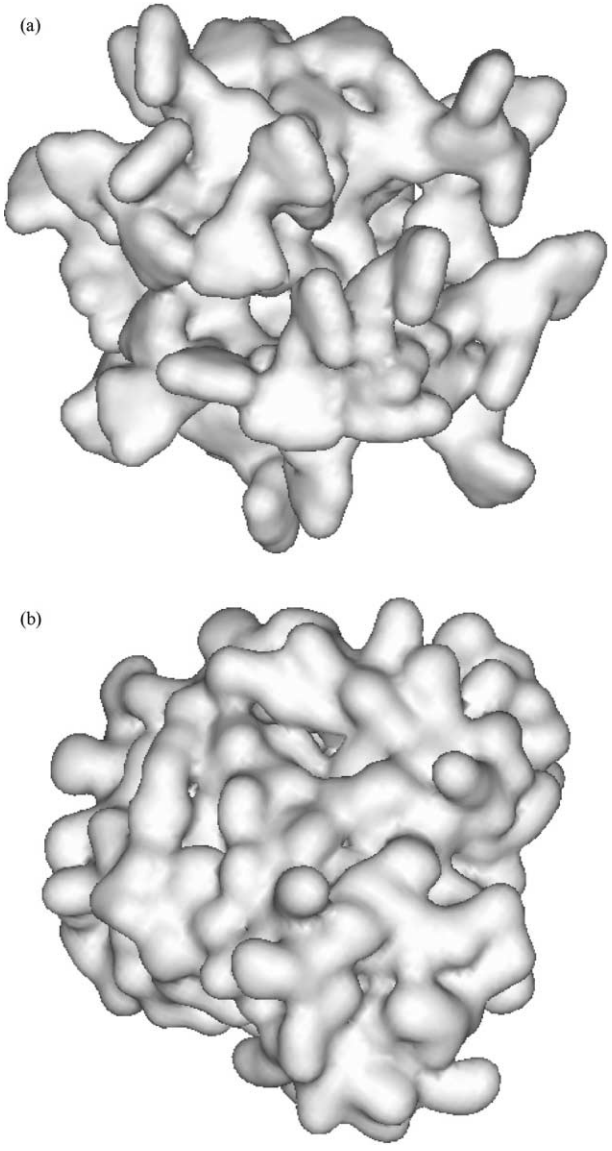

Figure 6. van der Waals molecular surfaces for G5 (a) and myoglobin (b).

To try to visualize this similarity of the two molecular systems, we report in Figure 6a the graphical representation of the van der Waals molecular surfaces obtained by the Connolly algorithm for the dendrimer G5 and for myoglobin (Fig. 6b), respectively.

As mentioned earlier, parameters such as size, shape and multiplicity are transcribed, and displayed throughout the dendrimer development. These variables can have dramatic effects on the ultimate shape, the interior topology and the exterior surface properties (alias congestion) of the developing dendrimer. Mathematically, we can appraise dendrimer surface congestion as a function of generation from the following relationship:

$$A_z = \frac{A_D}{N_Z} \propto \frac{R^2}{N_c N_b^G} \quad (3)$$

in which A_Z is the surface area per terminal group Z, A_D is the dendrimer surface area and N_Z is the number of terminal groups Z per generation.[4] From this relation we can see that, at higher generations G, the surface area per Z group should become increasingly smaller and experimentally approach the cross sectional area of the van der Waals dimension of the surface group Z. The generation G thus reached is referred to as the *starburst dense-packed (limited) generation*. As predicted by de Gennes and Hervet,[24] ideal starburst growth without branch defects is possible only for those generations preceding the dense-packed state. This critical dendrimer property gives rise to self-limiting starburst dimensions, which are a function of the branch-segment length l, the core multiplicity N_c, the branch-juncture multiplicity N_b and the sterical dimensions of the terminal group Z. Since the dendrimer radius R in the expression above is dependent of l, larger l values will delay this congestion, whereas larger N_c and N_b values and larger Z dimensions will dramatically hasten it.

Computer-assisted molecular simulations allowed us to determine the surface area per Z group, A_Z, as a function of generation (see Fig. 7). For the dendrimers with empty protoporphyrinic core, A_Z increases for generations 1–3, reaches a maximum at generation 4 and then, with G5, it begins to decline, owing to surface congestion. Quite a similar behavior seems to characterize other starburst molecules of different natures, such as poly(amido amine),[4] poly[propylene imine)[17] and poly(biphenyl-oxy-*n*-pentane).[25]

On the contrary, the dendrimers carrying a Fe–O_2–Hys complex coordinated to the protoporphyrin nucleus present a different behavior. In this case, the curve shows that A_Z monotonically decreases from generation 1 up to generation 5, although this decrement is confined to approximately 5%. This peculiar behavior can be sensibly ascribed to the combined effect of both the sterical hindrance of the amino acid and the increased number of detectable intramolecular H-bonds between the complex and the inner shells of the dendrimer. In fact, if the presence of hystidine accounts for an increased total surface area on one side, on the other the greater number of nonbonded interactions results in a more compact conformation of the dendrimeric branches, thus reducing the relative increment of the corresponding A_Z value.

Notwithstanding this different behavior, however, this analysis allows us to conclude that, for this type of dendrimers, the starburst limited generation, that is the generation at which the molecule should exhibit (1) sterically inhibited reaction rates, (2) sterically induced stoichiometry, and, quite possibly, (3) a critical phase change due to surface cooperativity (association) is presumably located in correspondence of G4, and that the presence of the biological complex within the protoporphyrinic nucleus does not modify the global behavior of the parent molecule.

The target of the subsequent detailed analysis of the energetic of both dendrimeric protoporphyrins is twofold: to evaluate the effect exerted by the dendrimer cage on the protoporphyrinic nucleus (either empty or complexed with Fe–O_2–Hys) and to characterize the class of molecules considered as a function of the generational level. As concerns the isolated dendrimers, the behavior exhibited by the energy components is that typical of these starburst polymers: the valence contribution (E_{val}) to the total potential energy (E_{pot}) monotonically increases with increasing G, whereas the nonbonded component (E_{nb}) decreases. Figure 8 reports, as an

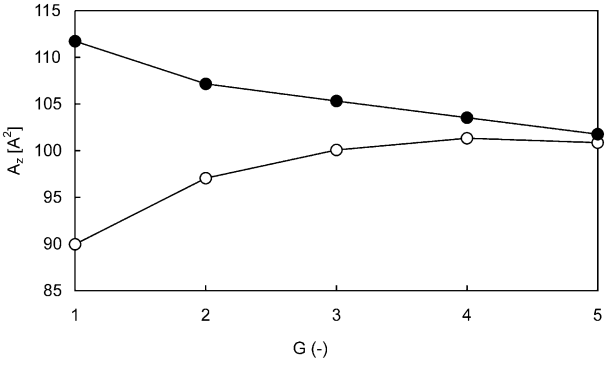

Figure 7. Surface area per terminal group versus generation for $dend_E$ (○) and $dend_C$ (●) (lines serve as guide for the eye).

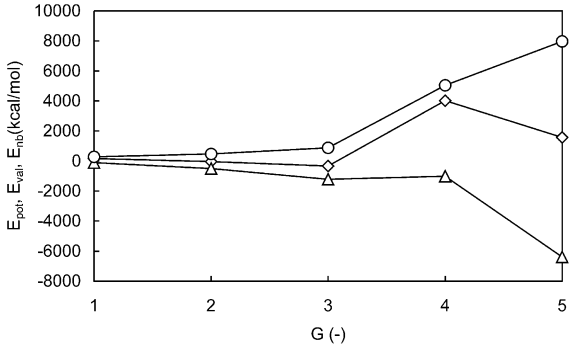

Figure 8. Potential energy E_{pot} and its components E_{val} and E_{nb} as obtained from equilibrium MD simulations for all five generations of $dend_E$ @ 298 K: E_{pot} (◇); E_{val} (○); E_{nb} (△) (lines serve as guide for the eye).

example, the plots of potential energy and its two major components as a function of the generational level for the $dend_E$. From this figure we can see how, at G4, the potential energy of the systems begins to increase, by virtue of the fact that the molecule has attained a densely packed, spherical conformation, and the already discussed phenomenon of surface congestion becomes manifest. The valence term increases according to the increasing number of atomic bonds, angles, torsions and inversions; the single behavior of each E_{val} subcomponent is reported in Figure 9. Here we may see that the bond term E_b undergoes the maximum increment, given the high degree of ramification that is observed as G is increased. The angle component of E_{pot}, E_a, exerts its major contribution at the lower generation levels; the insertion of the aromatic branch cells, in fact, implies that the connection bonds between the substituents and the core undergo a rotation in order to protrude from the plane of the protoporphyrinic nucleus and minimize the sterical repulsions. At the highest generation levels, due to the existing close packing conditions, the values of E_a still increases smoothly, since it is only slightly influenced by the overall molecular geometry variation. As expected, the torsional term E_t follows the same trend of E_a, whereas the contribution afforded by the inversion term E_i is almost negligible.

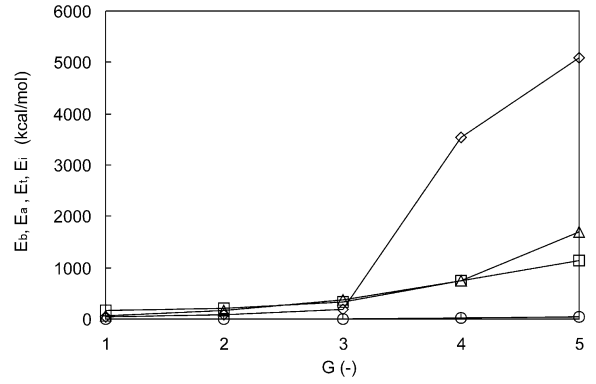

Figure 9. Valence energy term E_{val} and its components E_b, E_a, E_t and E_i as obtained from equilibrium MD simulations for all five generations of $dend_E$ @ 298K: E_b (◇); E_a (□); E_t (△); E_i (○) (lines serve as guide for the eye).

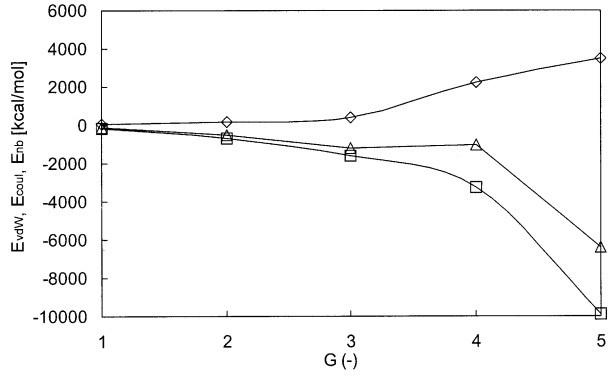

Figure 10. Nonbonded potential energy E_{nb} and its components E_{vdw} and E_{coul} as obtained from equilibrium MD simulations for all five generations of $dend_E$ @ 298 K: E_{nb} (△); E_{vdw} (◇); E_{coul} (□) (lines serve as guide for the eye).

The nonbonded energy term, as defined in the Universal Force Field,[26] is given by the sum of the van der Waals (E_{vdw}) and the Coulombic (E_{coul}) contributions. The value of E_{vdw} for each dendrimer generation is always positive and increasing, to indicate that, as the structure of the dendrimer becomes more and more tangled, the repulsive component prevails over the dispersive one; on the contrary, as G increases, the molecules progressively stabilizes its electrostatic interactions. From Figure 10, we can also argue that the two nonbonded components of potential energy no do show the same rate of increase. Indeed, the increment in the Coulomb term is always greater than that due to van der Waals, exception made for the conformational transition region between G3 and G4 (already highlighted by the ratio of the inertia axes in Fig. 3).

The insertion of the complex Fe–O_2–Hys, once again, does not result in an appreciable modification of the qualitative energetic behavior of this molecular series. Both the bond and the nonbonded components of the potential energy present a difference in modulus with respect to the base dendrimer molecule as an obvious consequence of the augmented number of atoms in the system. For the earlier generations (G1 and G2), this difference is slightly more marked in the case of the complexed protoporphyrinic nucleus but, as the generational growth proceeds, this difference is smoothed out so that an energetic differentiation between the two molecular series is no longer possible (suffice here to consider that, in case of G4 for instance, the relative weight of the complex Fe–O_2–Hys over the total number of atom is about 3%).

The second part of the energetic evaluation concerns a situation, which might be considered, although necessarily in a rough and simplified manner, representative of an aqueous environment. As expected, the trend of the valence term of E_{pot} parallels that exhibited by the molecule in vacuum, except for a quantitative shift due to the highly increased total number of atoms. On the contrary, major differences can be observed in the behavior of the nonbonded energy term E_{nb} and its components, E_{vdw} and E_{coul}. Figure 11 compares the curves of these terms, as a function of the dendrimer generation, for the isolated molecule and that

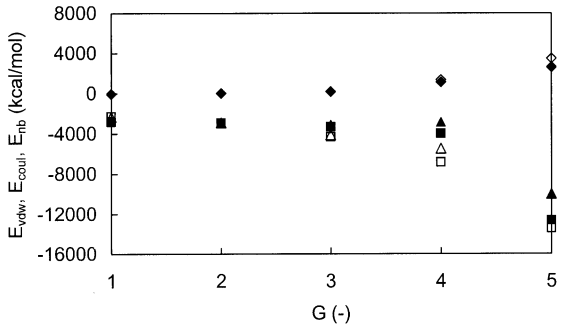

Figure 11. Comparison between the nonbonded potential energy components for the $dend_E$ generations in vacuum (open symbols) and in water (filled symbols): E_{nb} (triangles); E_{vdw} (diamonds); E_{coul} (squares).

surrounded by the aqueous environment. As we may understand, the electrostatic component is positively influenced by the presence of the water solvent, as the formation of a network of hydrogen bonds is detected between the starburst molecule and water at each dendrimer generation. We can then conclude that the presence of a polar solvated environment stabilizes the dendrimeric series; as a consequence of this, the sharp energy variation between G3 and G4 observed for the molecule in vacuum is smoothed out in water.

Once again, the presence of the Fe–O_2–Hys complex in the protoporphyrinic nucleus does not seem to influence the features observed for the dendrimer with an empty nucleus; this allows us definitely to conclude that, by virtue of these evidences and the experimental findings that these substances display reversible dioxygen-binding activity, in which the dioxygen adduct survives over a period of months even in the presence of water,[9] they could be eventually exploited as the first dendrimer-based monomolecular model of hemoproteins, which affords a long-lived dioxygen adduct due to the sterical, hydrophobic and electrostatic protection of the active site.

Computational Details

All simulation were run on a Silicon Graphics Origin 200 (microprocessor MIPS RISC 10000, 64 bit CPU, 512 MB RAM) and performed by using the commercial software *Cerius*[2] (v. 4.2) from Accelrys Inc. (for both molecular mechanics (MM) and molecular dynamics (MD) simulation) and in-house developed codes, standalone or implemented in the commercial package.

The generation of molecular accurate model structures was conducted as follows. For each dendrimer generation, the molecule was built and its geometry optimized via energy minimization using the Universal force field (UFF, v. 1.02).[26] This UFF has a set of fundamental parameters, based only on the element, its hybridization, and its connectivity. In particular, the parameters used in Universal FF include a set of hybridization-dependent atomic bond radii, a set of hybridization angles, van der Waals parameters, torsional and inversion barriers, and a set of effective nuclear charges. The elements in the UFF periodic table are the atom types: atom of the same type may only be similar chemically and physically, yet as is the norm, they are treated identically in the force field.

All the molecules were modeled to have a total charge equal to zero, and the distribution of the partial charge within each molecule was determined by the charge equilibration method of Rappé et al.[27] Energy was minimized by up to 5000 Newton–Raphson iterations. Following this procedure, the root-mean-square (rms) atomic derivatives in the low energy regions were smaller than 0.05 kcal/mol Å. Long-range nonbonded interactions were treated by applying suitable cutoff distances, and to avoid the discontinuities caused by direct cutoffs, the cubic spline switching method was used. Van der Waals distances and energy parameters for nonbonded interactions between heteronuclear atoms were obtained by the 6th-power combination rule proposed by Waldman and Hagler.[28] Such a straightforward molecular mechanics scheme is likely to trap the simulated system in a metastable local high-energy minimum. To prevent the system from such entrapments, the relaxed structures were subjected to simulated annealing (five repeated cycles from 298 to 1000 K and back) using constant volume/constant temperature molecular dynamics conditions.[29,30] At the end of each annealing cycle, the structures were again relaxed via FF, using the same convergence criteria described above.

The calculation of molecular surfaces was performed using the so-called Connolly dot surfaces algorithm.[31,32] Accordingly, a probe sphere of given radius p_r, representing the solvent molecule, is placed tangent to the atoms of the molecule at thousands different position. For each position in which the probe does not experience van der Waals overlap with the atoms of the molecule, points lying on the inward-facing surface of the probe sphere become part of the molecule *solvent-accessible surface* (S_{AS}). According to this procedure, the molecular surface generated consists of the van der Waals surface of the atoms which can be touched by a solvent-sized probe sphere (thus called *contact surface*), connected by a network of concave and saddle surfaces (globally called *reentrant surface*), that smoothes over crevices and pits between the atoms of the molecule. The sum of the contact and the reentrant surface forms the so-called *molecular surface* (MS); this surface is the boundary of the *molecular volume* (M_r) that the solvent probe is excluded from if it is not to undergo overlaps with the molecule atoms, which therefore is also called *solvent-excluded volume*. Finally, performing the same procedure by setting the probe sphere radius equal to zero, the algorithm yields the *van der Waals surface* (WS).

The details of the isolated dendrimer structures at 298 K were obtained by performing MD simulations under isocoric/isothermal (NVT) conditions. For the calculation of the molecular properties in the aqueous environment, each dendrimer molecule was confined, together with 512 water molecules, in a cubic box with periodic boundary conditions (PBC). Each water molecule was modeled by a simple three-point charge (SPC) model, which has been verified to satisfactorily describe the properties of bulk water at ordinary temperatures.[33] In order to minimize the artifact of periodicity, a cutoff distance was set equal to half the box length. The resultant structures were relaxed via MM, again using UFF; in this case, the Ewald technique was employed in handling nonbonded interactions. Further, to limit the effects due to a peculiar distribution of the water molecules in the cubic box, ten independent structures for each dendrimeric generation considered in this study were generated according to the procedure described above. The properties reported below are then to be considered as ensemble averaged from the appropriate set of 10 structures.

Each molecular dynamics run was started by assigning initial velocity for atoms according to Boltzmann distribution at 2×T. Temperature was controlled via weak coupling to a temperature bath,[34] with coupling constant $\tau_T = 0.01$ ps. The Newton molecular equations of motion were solved by the Verlet leapfrog algorithm,[35] using an integration step of 1 fs. Since the partial charges assigned by the charge equilibration method are dependent on structure geometry, they were updated regularly every 100 MD steps during the entire MD runs.

Each MD simulation consisted in a system equilibration phase, during which the equilibration process was followed by monitoring the time evolution of both the kinetic and potential energy, and a successive data collection phase. Almost in all case, the energy components have ceased to show a systematic drift and have started to oscillate about steady mean values around 40–50 ps. Accordingly, equilibration phases longer than 100 ps and data acquisition runs longer than 500 ps were judged not necessary to enhance data accuracy.

Acknowledgements

This work was supported by the Ministero Italiano per l'Università e la Ricerca (MIUR, Rome, Italy) and by the University of Trieste, Italy (special grant for scientific research to S.P. and M.F.).

References and Notes

1. Frechét, J. M. J.; Hawker, C. J. Synthesis and Properties of Dendrimers and Hyperbranched Polymers, In Aggarwal, S. L., Russo, S., Eds.; *Comprehensive Polymer Science*; Elsevier: Oxford, 1996; p 140.
2. Matthews, O. A.; Shipway, A. N.; Stoddart, J. F. *Prog. Polym. Sci.* **1998**, 231.
3. Newkome, G. R.; Moorefield, C. N.; Vögtle, F. *Dendritic Molecules: Concepts, Syntheses, Perspectives*; VCH Verlaggesellschaft: Weinhein, 1996.
4. Tomalia, D. A.; Naylor, A. M.; Goddard, W. A., III *Angew. Chem. Intl. Ed. Engl.* **1990**, *29*, 138.
5. Cram, D. J. *Angew. Chem., Int. Ed. Engl.* **1988**, *27*, 1009.
6. Lehn, J. M. *Angew. Chem., Int. Ed. Engl.* **1988**, *27*, 90.
7. Amit, A. G.; Mariuzza, A. R.; Phillips, S. E. V.; Poljak, R. J. *Science* **1986**, *233*, 7074.
8. Lewis, M.; Rees, D. C. *Science* **1985**, *230*, 1163.
9. Jiang, D. L.; Aida, T. *J. Chem. Soc., Chem. Commun.* **1996**, 1523.
10. Almong, J.; Baldwin, J. E.; Huff, J. *J. Am. Chem. Soc.* **1975**, *97*, 227.
11. Collman, J. P.; Brauman, J. I.; Collins, T. J.; Iverson, B. L.; Pettman, R. B.; Sessler, J. L.; Walters, M. A. *J. Am. Chem. Soc.* **1983**, *105*, 3038.
12. Collman, J. P.; Gange, R. R.; Reed, C. A.; Halbert, T. R.; Lang, G.; Robinson, W. T. *J. Am. Chem. Soc.* **1975**, *97*, 1427.
13. Momenteau, M.; Reed, C. A. *Chem. Rev.* **1994**, *94*, 659.
14. Ward, B.; Wang, C. B.; Chang, C. K. *J. Am. Chem. Soc.* **1981**, *103*, 5236.
15. Tsuchida, E.; Komatsu, T.; Arai, K.; Nishide, H. *J. Chem. Soc. Dalton Trans.* **1993**, 2465.
16. Jin, R. H.; Aida, T.; Inoue, S. J. *Chem. Commun.* **1996**, 1523.
17. Blasizza, E.; Fermeglia, M.; Pricl, S. *Mol. Simul.* **2000**, *24*, 167.
18. Naylor, A.; Goddard, W. A., III; Kiefer, G. E.; Tomalia, D. A. *J. Am. Chem. Soc.* **1989**, *111*, 2339.
19. Birdi, K. S. *Fractals in Chemistry, Geochemistry and Biophysics*; Plenum Publishing Corporation: New York, 1993.
20. Suwa, N.; Takahashi, T. *Morphological and Morphometrical Analysis of Circulation in Hypertension and Ischemic Kidney*; Urban & Schwarzenberg: Munich, 1971.
21. Mandelbrot, B. B. *The Fractal Geometry of Nature*; Freeman: San Francisco, 1983.
22. Phillips, S. E.; Schoenborn, B. P. *Nature* **1981**, *292*, 81.
23. Berman, H. M.; Westbrook, J.; Feng, Z.; Gilliland, G.; Bhat, T. N.; Weissig, H.; Shindyalov, I. N.; Bourne, P. *E; Nucl. Acids Res.* **2000**, *28*, 235.
24. de Gennes, P. G.; Hervet, H. J. *Phys. Lett.* **1983**, *44*, 351.
25. Gelmetti, S.; Fermeglia, M.; Pricl, S. *Proceedings of the* AIChE Annual Meeting, Reno, NV, USA, Nov 4–9, 2001.
26. Rappè, A. K.; Casewitt, C. J.; Colwell, K. S.; Goddard, W. A., III; Skiff, W. M. *J. Am. Chem. Soc.* **1992**, *114*, 10024.
27. Rappé, A. K.; Goddard, W. A., III *J. Phys. Chem.* **1991**, *95*, 3358.
28. Waldmann, M.; Hagler, A. T. *J. Comput. Chem.* **1993**, *14*, 1077.
29. Pricl, S.; Fermeglia, M. *Carbohydr. Polym.* **2001**, *45*, 23.
30. Fermeglia, M.; Pricl, S. *AIChE J.* **1999**, *45*, 2619.
31. Connolly, M. L. *J. Appl. Crystallogr.* **1983**, *16*, 548.
32. Connolly, M. L. *J. Am. Chem. Soc.* **1985**, *107*, 1118.
33. Berendsen, H. J. C.; Postma, J. P. M.; Di Nola, A.; van Gunsteren, W. F.; Haak, J. R. *J. Chem. Phys.* **1984**, *81*, 3684.
34. Andersen, H. C. *J. Chem. Phys.* **1980**, *72*, 2384.
35. Verlet, L. *Phys. Rev.* **1967**, *159*, 98.